Journal of Marine Science and Technology

Volume 20 | Issue 5 Article 16

DESIGN AND IMPLEMENTATION OF AN SIMULATION OF WATER WAVE TRANSFORMATION USING HIGHER ORDER MILD-SLOPE EQUATION

Yuan-Jyh Lan
Research Center for Ocean Energy and Strategies, National Taiwan Ocean University, Keelung, Taiwan, R.O.C.

Tai-Wen Hsu
Research Center for Ocean Energy and Strategies, National Taiwan Ocean University, Keelung, Taiwan, R.O.C.
Department of Hydraulic and Ocean Engineering, National Cheng Kung University, Tainan, Taiwan, R.O.C.

Ta-Yuan Lin
Department of Hydraulic and Ocean Engineering, National Cheng Kung University, Tainan, Taiwan, R.O.C.

Shin-Jye Liang
Department of Marine Environmental Informatics, National Taiwan Ocean University, Keelung, Taiwan, R.O.C., sjliang@ntou.edu.tw

Recommended Citation

Lan, Yuan-Jyh; Hsu, Tai-Wen; Lin, Ta-Yuan; and Liang, Shin-Jye (2012) "DESIGN AND IMPLEMENTATION OF AN SIMULATION OF WATER WAVE TRANSFORMATION USING HIGHER ORDER MILD-SLOPE EQUATION," *Journal of Marine Science and Technology*: Vol. 20: Iss. 5, Article 16.
DOI: 10.6119/JMST-012-0905-1
Available at: https://jmstt.ntou.edu.tw/journal/vol20/iss5/16

DESIGN AND IMPLEMENTATION OF AN SIMULATION OF WATER WAVE TRANSFORMATION USING HIGHER ORDER MILD-SLOPE EQUATION

Acknowledgements

This research was supported by the National Science Council under grant number NSC96-2221-E-006-061, Taiwan, and in part by the Landmark Project of National Cheng Kung University, Taiwan.

Journal of Marine Science and Technology, Vol. 20, No. 5, pp. 603-611 (2012)
DOI: 10.6119/JMST-012-0905-1

DESIGN AND IMPLEMENTATION OF AN SIMULATION OF WATER WAVE TRANSFORMATION USING HIGHER ORDER MILD-SLOPE EQUATION

Yuan-Jyh Lan[1], Tai-Wen Hsu[1,2], Ta-Yuan Lin[2], and Shin-Jye Liang[3]

Key words: wave transformation, high-order, mild-slope equation, Boussinesq equations.

ABSTRACT

A higher-order mild-slope equation (HOMSE) is derived based on theory of Hsu *et al*. [14]. Depth function is approximated up to third-order accurate in terms of both wave nonlinearity and bottom slope. Classical Galerkin method is used to solve HOMSE. Developed model is verified with a series of benchmark tests, including propagation of a sinusoidal wave past a submerged bar, wave propagating on a sloping bed, wave propagating over an elliptic shoal on a uniform slope, and wave propagating through a semicircular slope bottom, respectively. Computed results are compared with experiment data and prediction of low-order mild-slope equation model as well as Boussinesq equations model, and show good agreement.

I. INTRODUCTION

The combined effect of wave refraction and diffraction can be described by the mild-slope equation (MSE) that was first derived for the two horizontal dimensions by Berkhoff [2]. The depth average MSE is derived from the following

$$\int_{-h}^{0} f_0 \left(\nabla_h^2 \Phi + \Phi_{zz} \right) dz = 0 \tag{1}$$

where $\Phi(x, y, z, t) = f_0(z, h)\phi(x, y, t)$ is the velocity potential, f_0 the depth function, $\nabla_h = (\partial/\partial x, \partial/\partial y)$ the horizontal gradient operator, $h(x, y)$ the arbitrary water depth, x, y and z are horizontal offshore, alongshore and vertical directions, and t the time, respectively. In accordance with the locally constant depth (or mild-slope) assumption, the depth function is obtained from linear wave theory given by

$$f_0(z,h) = \frac{\cosh k(z+h)}{\cosh kh} \tag{2}$$

where k is the wavenumber. Note that f_0 is only legitimate for a flat bottom.

Upon substituting Eq. (2) into Eq. (1), the time invariant MSE can be written as

$$\nabla_h \cdot \left(CC_g \nabla_h \phi \right) + k^2 CC_g \phi = 0 \tag{3}$$

Eq. (3) is the classical MSE with the mild-slope assumption $\left|\nabla_h h\right| / kh << 1$.

If the mild-slope assumption is not made, then the second-order terms of bottom effect ($\nabla_h^2 h$ and $\left|\nabla_h h\right|^2$) are retained. Chamberlain and Porter [6] developed a modified mild-slope equation (MMSE). Their computation results show that the MMSE provides more accurate for ramp of Booij [5] and laboratory measurements for sinusoidal bottom undulations conducted by Davies and Heathershow [11].

It is important for the perspective to recall that MSE is only valid for the cases of locally constant depth and linear waves. Considering the extreme conditions, it is natural to ask how well the assumption is satisfied. Since the vanish of the horizontal normal vector on a sloping bottom is neither appropriate nor realistic [14]. One way to remedy the limitation of classic mild-slope equation is to include effect of vertical variation of the motion given by f_0 in Eq. (2).

Another approach is the derivation of the 1D MSE by Svendsen [20] which is based on the analytical solution of wave motion on a sloping bottom by Biesel [4]. Their solution

Paper submitted 04/10/12; revised 09/04/12; accepted 09/05/12. Author for correspondence: Shin-Jye Liang (e-mail: sjliang@ntou.edu.tw).
[1] *Research Center for Ocean Energy and Strategies, National Taiwan Ocean University, Keelung, Taiwan, R.O.C.*
[2] *Department of Hydraulic and Ocean Engineering, National Cheng Kung University, Tainan, Taiwan, R.O.C.*
[3] *Department of Marine Environmental Informatics, National Taiwan Ocean University, Keelung, Taiwan, R.O.C.*

includes velocity potential proportional to $|\nabla_h h|$ which corresponds to the higher-order terms of MMSE. However, the derivation does not include the bottom slope $|\nabla_h h|$ and curvature term $\nabla_h^2 h$. A complementary mild-slope equation (CMSE) is derived by Hsu *et al*. [14] for describing waves propagating over a sloping bottom. CMSE introduces a new depth function in which analytical solution with the linear wave amplitude is implemented [9]. The CMSE adopts the second-order solution of Chen *et al*. [9] which includes bottom slope and wave refraction of obliquely incident waves. The numerical results show that the CMSE provides a significant improvement in simulation ramp of Booij [5] and reflection coefficient of Bragg scattering on an undulated bottom. However, wave nonlinearity and frequency dispersion are not included in the CMSE. Therefore, CMSE is limited in some situations, for example, in a shallow water region where the effects of nonlinearity and frequency dispersion becomes significant.

An alternate is to apply Boussinesq equations (BE) [12, 18, 22] to provide an accurate description of wave nonlinear and dispersive transformations in the nearshore regions. In addition to computation of wave field, nearshore wave-induced currents, mean water level variation, interactions of wave-wave and wave-current can also be incorporated in the BE model. Although, BE models can predict wave transformation with acceptable accuracy, their applicability and effectiveness still remain the possibility to develop an efficient nonlinear wave model.

In this paper, a higher-order mild-slope equation (HOMSE) is developed based on theory of Chen *et al*. [9], in which the depth functions are expressed in terms of the combined effect of nonlinearity, dispersion and bottom slope. We extend method of Hsu *et al*. [14] to third-order accuracy in terms of nonlinearity as well as slope and curvature of bottom. The model is validated with a series of benchmark tests where wave travelling over various slope bottoms. The effects of nonlinearity and frequency dispersion on HOMSE are systematically analyzed and discussed.

II. TEORETICAL DEVELOPMENT

In the theoretical formulation, we expand all quantities in a power series in two parameters ε and α, where $\varepsilon = ka$ denotes the wave nonlinearity, a is the wave amplitude, and α is the bottom slope of an arbitrary bottom configuration. The expression of the velocity potential Φ and wavenumber k in terms of ε and α [9] are, respectively,

$$\begin{aligned}\Phi &= \sum_{i=1}^{\infty}\sum_{j=0}^{\infty}\varepsilon^i\alpha^j\Phi_{ij}\\ &= \varepsilon\ (\Phi_{10}+\alpha\Phi_{11}+\alpha^2\Phi_{12}+...)\\ &\quad +\varepsilon^2(\Phi_{20}+\alpha\Phi_{21}+....)+\varepsilon^3(\Phi_{30}+....)\end{aligned} \tag{4}$$

$$\begin{aligned}\eta &= \sum_{i=1}^{\infty}\sum_{j=0}^{\infty}\varepsilon^i\alpha^j\eta_{ij}\\ &= \varepsilon\ (\eta_{10}+\alpha\eta_{11}+\alpha^2\eta_{12}+...)\\ &\quad +\varepsilon^2(\eta_{20}+\alpha\eta_{21}+....)+\varepsilon^3(\eta_{30}+....)\end{aligned} \tag{5}$$

$$\begin{aligned}k &= \sum_{m=0}^{\infty}\sum_{n=0}^{\infty}\varepsilon^m\alpha^n k_{mn}\\ &= \varepsilon^0 k_{00}+\varepsilon(k_{10}+\alpha k_{11}+\alpha^2 k_{12}+....)\\ &\quad +\varepsilon^2(k_{20}+\alpha k_{21}+....)+\varepsilon^3(k_{30}+....)\end{aligned} \tag{6}$$

where the velocity potential Φ is expressed by different orders as follows

$$\Phi_{10}=\phi_{10}\ \ f_{10}=\frac{ag}{\omega}\frac{\mathrm{ch}\,k(h+z)}{\mathrm{ch}\,kh}\sin S \tag{7}$$

$$\begin{aligned}\Phi_{11} &= \phi_{11}\ \ f_{11}\\ &= \frac{ag}{\omega}\left\{\left[-\frac{k^2(h+z)^2}{D\,\mathrm{sh}\,2kh}+k(h+z)\right]\frac{\mathrm{ch}\,k(h+z)}{\mathrm{ch}\,kh}\right.\\ &\quad \left.-\frac{k(h+z)}{D^2\,\mathrm{th}\,kh}\frac{\mathrm{sh}\,k(h+z)}{\mathrm{ch}\,kh}\right\}\cos S\end{aligned} \tag{8}$$

$$\begin{aligned}\Phi_{12} &= \phi_{12}\ \ f_{12}\\ &= \frac{ag}{\omega}\left\{\left[-\frac{k^4(h+z)}{2(D\,\mathrm{sh}\,2kh)^2}+\frac{k^3(h+z)^3}{D\,\mathrm{sh}\,2k_0h}-\frac{(D^4-4D+5I^2)}{2D^4}k^2(h+z)^2\right.\right.\\ &\quad \left.+\frac{Ik(h+z)}{D^2}\right]\frac{\mathrm{ch}\,k(h+z)}{\mathrm{ch}\,kh}\\ &\quad +\left[-\frac{4D+10\,\mathrm{ch}^2\,k_0h}{3D^3\,\mathrm{sh}^2\,2k_0h}k^3(h+z)^3+\frac{2\left(D+\mathrm{ch}^2\,kh\right)}{D^2\,\mathrm{sh}\,2kh}k^2(h+z)^2\right.\\ &\quad \left.\left.-(k-k_2)(h+z)\right]\frac{\mathrm{sh}\,k(h+z)}{\mathrm{ch}\,kh}\right\}\sin S\end{aligned} \tag{9}$$

$$\Phi_{20}=\phi_{20}\ \ f_{20}=\frac{3}{8}\omega a^2\frac{\mathrm{ch}\,2k(h+z)}{\mathrm{sh}^4\,kh}\sin 2S \tag{10}$$

$$\begin{aligned}\Phi_{21} &= \phi_{21}f_{21}\\ &= \omega a^2\left\{\left[-\frac{3(I^4-1)k^2(h+z)}{4D\,\mathrm{sh}\,2kh}+\frac{3(I^2+1)k(h+z)}{4\,\mathrm{sh}^4\,kh}\right.\right.\\ &\quad -(I^2+1)(12D^2I^6+(6D^2+3D)I^5-(48D-24D)I^4\\ &\quad -(18D^2+2D-22)I^3+(36D^2-24D)I^2\\ &\quad \left.-(D+10)I)/(16D^2)\right]\times\frac{\mathrm{ch}\,2k(h+z)}{\mathrm{ch}\,2kh}\\ &\quad \left.-\frac{3[2D(I^4-1)+(D+1)(I^3+1)]}{4D^2\,\mathrm{sh}^2\,kh}k(h+z)\frac{\mathrm{sh}\,2k(h+z)}{\mathrm{ch}\,2kh}\right\}\cos 2S\end{aligned} \tag{11}$$

$$\begin{aligned}\Phi_{30} &= \phi_{30} f_{30} \\ &= \omega k a^3 (9I^7 + 5I^5 - 53I^3 + 39I)\frac{\mathrm{ch}\,3k(h+z)}{\mathrm{ch}\,3kh}\sin 3S \\ &\quad + \frac{\omega k_{30} a}{k}(h+z)\frac{\mathrm{sh}\,k(h+z)}{\mathrm{sh}\,kh}\sin S\end{aligned} \tag{12}$$

where sh = sinh, ch = cosh, th = tanh, I = coth kh, $D = 1 + 2kh/\mathrm{sh}\,2kh$, $k_{30} = (k/3D^5)[D^5 + (D^4 - 18D^2 + 32\mathrm{D} - 15)\mathrm{ch}^2\,kh + 2D^2 + (-3D^2 + 15D - 15)I^2]$, and $S = k\vec{r} - \omega t$ is the phase function.

Notably we leave ω unexpanded to meet an argument to the trigonometric functions. Substituting the above equations into the integral equation of Eq. (1) and replacing f_0 by f_{ij}, we collect corresponding terms proportional to the same order, the following approximations in MSE are thus obtained:

$$\begin{aligned}&O(\varepsilon\alpha^0): \\ &-\frac{\partial^2\phi_{10}}{\partial t^2} + \nabla_h\cdot(CC_g\nabla_h\phi_{10}) \\ &+\left[k^2CC_g - \omega^2 + f_1 g\nabla_h^2 h + f_2\left|\nabla_h h\right|^2 gk\right]\phi_{10} = 0\end{aligned} \tag{13}$$

$$\begin{aligned}&O(\varepsilon\alpha): \\ &-\frac{1}{g}\frac{\partial^2\phi_{11}}{\partial t^2}E_{11} + \nabla_h\cdot(A_{11}\nabla_h\phi_{11}) \\ &+\left(B_{11} + C_{11}\nabla_h^2 h + D_{11}\left|\nabla_h h\right|^2 - F_{11}\right)\phi_{11} = 0\end{aligned} \tag{14}$$

$$\begin{aligned}&O(\varepsilon\alpha^2): \\ &-\frac{1}{g}\frac{\partial^2\phi_{12}}{\partial t^2}E_{12} + \nabla_h\cdot(A_{12}\nabla_h\phi_{12}) \\ &+\left(B_{12} + C_{12}\nabla_h^2 h + D_{12}\left|\nabla_h h\right|^2 - F_{12}\right)\phi_{12} = 0\end{aligned} \tag{15}$$

$$\begin{aligned}&O(\varepsilon^2\alpha^0): \\ &-\frac{1}{g}\frac{\partial^2\phi_{20}}{\partial t^2}E_{20} + \nabla_h\cdot(A_{20}\nabla_h\phi_{20}) \\ &+\left(B_{20} + C_{20}\nabla_h^2 h + D_{20}\left|\nabla_h h\right|^2 - F_{20}\right)\phi_{20} \\ &+E_{20}(\nabla_h\phi_{10}\cdot\nabla_h\eta_{10}) = 0\end{aligned} \tag{16}$$

$$\begin{aligned}&O(\varepsilon^2\alpha): \\ &-\frac{1}{g}\frac{\partial^2\phi_{21}}{\partial t^2}E_{21} + \nabla_h\cdot(A_{21}\nabla_h\phi_{21}) \\ &+\left(B_{21} + C_{21}\nabla_h^2 h + D_{21}\left|\nabla_h h\right|^2 - F_{21} - J_{21}\right)\phi_{21} \\ &+G_{21}(\nabla_h\phi_{10}\cdot\nabla_h\eta_{10}) + H_{21}(\nabla_h\phi_{11}\cdot\nabla_h\eta_{10}) \\ &+I_{21}(\nabla_h\phi_{11}\cdot\nabla_h\eta_{10}) - K_{21}\nabla_h\phi_{20} - L_{21}\phi_{20} = 0\end{aligned} \tag{17}$$

$$\begin{aligned}&O(\varepsilon^3\alpha^0): \\ &-\frac{1}{g}\frac{\partial^2\phi_{30}}{\partial t^2}E_{30} + \nabla_h\cdot(A_{30}\nabla_h\phi_{30}) \\ &+\left(B_{30} + C_{30}\nabla_h^2 h + D_{30}\left|\nabla_h h\right|^2 - F_{30}\right)\phi_{30} \\ &+G_{30}(\nabla_h\phi_{10}\cdot\nabla_h\eta_{20}) + H_{30}(\nabla_h\phi_{20}\cdot\nabla_h\eta_{10}) \\ &+I_{30}(\phi_{20}\nabla_h\eta_{10}) = 0\end{aligned} \tag{18}$$

where f_1, f_2, A_{ij}, B_{ij}, C_{ij}, D_{ij}, E_{ij}, F_{ij}, G_{ij}, H_{ij}, I_{ij}, J_{ij}, $i, j = 0, 1, 2$ are corresponding coefficients which are in terms of functions of the dispersion parameter kh. Detailed derivations and expressions of the coefficients are referred to Lin [17]. Following the procedure outlined by Hsu *et al.* [14], a slow varying coordinate of the time variable is introduced, and the following relationships are assumed, $\bar{t} = \xi t$ and $\phi_{mn} = \psi_{mn}(x, y, \bar{t})e^{m(-i\omega t)}$, where ξ is a perturbation parameter of the order $\left|\nabla_h h\right|/kh$, m represents the order of the nonlinearity, and n denotes the order of the bottom slope, $\psi_{mn} = \varphi_{mn}/\sqrt{A_{mn}}$ is the Liouville transformation proposed by Radder [19], A_{mn} is the coefficient of the velocity coefficient in the order of $\varepsilon^m\alpha^n$, respectively. Substitution of these expressions into Eqs. (13)-(18), one can obtain

$$\frac{-2im\omega}{A_{mn}}\frac{\partial\varphi_{mn}}{\partial t} = \nabla_h^2\varphi_{mn} + k_{cmn}^2\varphi_{mn} + RHS_{mn} \tag{19}$$

where k_{cmn} is a pseudo wavenumber given by

$$\begin{aligned}k_{cmn}^2 &= \left(B_{mn} + C_{mn}\nabla_h^2 h + D_{mn}\left|\nabla_h h\right|^2 - F_{mn} + m^2\omega^2/gE_{mn}\right)\Big/A_{mn} \\ &\quad - \nabla_h^2\sqrt{A_{mn}}\Big/\sqrt{A_{mn}}\end{aligned} \tag{20}$$

and RHS_{mn} denotes the additional terms in each order, as presented in Table 1.

Here the radiation boundary condition is specified to reduce the reflection of waves back into the study domain. Three types of radiation boundary conditions are considered: a full or partial reflection boundary condition, and a given boundary condition [15].

1. Open boundary condition

$$\frac{\partial\varphi}{\partial x} = i\bar{\alpha}k\left[1 + \frac{1}{2k^2}\frac{\partial^2\varphi}{\partial y^2} - \frac{1}{8k^4}\frac{\partial^4\varphi}{\partial y^4}\right] \tag{21}$$

$$\frac{\partial\varphi}{\partial y} = i\bar{\alpha}k\left[1 + \frac{1}{2k^2}\frac{\partial^2\varphi}{\partial x^2} - \frac{1}{8k^4}\frac{\partial^4\varphi}{\partial x^4}\right] \tag{22}$$

Table 1. Additional term RHS_{mn} of each order in Eq. (19).

Order	RHS_{mn}
$O(\varepsilon\alpha^0)$	0
$O(\varepsilon\alpha)$	0
$O(\varepsilon\alpha^2)$	0
$O(\varepsilon^2\alpha^0)$	$-E_{20}(\nabla_h\phi_{10}\cdot\nabla_h\eta_{10})$
$O(\varepsilon^2\alpha)$	$-\left[G_{21}(\nabla_h\phi_{10}\cdot\nabla_h\eta_{10})+H_{21}(\nabla_h\phi_{11}\cdot\nabla_h\eta_{10})+I_{21}(\nabla_h\phi_{11}\cdot\nabla_h\eta_{10})-K_{21}\nabla_h\phi_{20}-L_{21}\phi_{20}\right]$
$O(\varepsilon^3\alpha^0)$	$-\left[G_{30}(\nabla_h\phi_{10}\cdot\nabla_h\eta_{20})+H_{30}(\nabla_h\phi_{20}\cdot\nabla_h\eta_{10})+I_{30}(\phi_{20}\nabla_h\eta_{10})\right]$

Table 2. Incident wave condition and still water depth of experiment of Beji *et al*. [1].

Case	T (sec)	H (m)	h/L	H/L	U_r
case 1	1.25	0.025	0.1951	0.012	1.64

where $\bar{\alpha} = (1 - R)/(1 + R)$ is the absorption coefficient, and R is the reflection coefficient. When $\bar{\alpha} = 0$ and $\bar{\alpha} = 1$, the above boundary condition represents total reflection and total passing through boundary, respectively.

2. Lateral boundary condition

$$\frac{\partial\phi}{\partial y}(x, y_0) = 0, \quad \frac{\partial\phi}{\partial y}(x, y_p) = 0 \tag{23}$$

$$\frac{\partial^3\phi}{\partial y^3}(x, y_0) = 0, \quad \frac{\partial^3\phi}{\partial y^3}(x, y_p) = 0 \tag{24}$$

3. Given boundary condition
   For a given nonlinear incident wave height H, period T, and incident wave angle θ_0, the velocity potential is given by theory of Chen *et al*. [7, 8].

III. MODEL VERIFICATIONS AND APPLICATIONS

Developed HOMSE model is verified against a series of benchmark tests, and computed results are compared with experiment data and/or results of other numerical models, such as low-order mild-slope equation (MSE) model and Bousinessq equations (BE) model, in this section.

1. Wave Past A Submerged Bar

HOMSE is used to simulate wave propagation over a submerged breakwater and computed results are compared with experiment data of Beji *et al*. [1]. The input wave conditions are summarized in Table 2, where U_r denotes the Ursell number measuring the nonlinearity of incident waves $(U_r = H_0 L_0^2 / h^3)$. Fig. 1 shows the bathymetry of the submerged bar. Comparison of computed results and laboratory observations is illustrated in Fig. 2. It depicts wave height variations around the submerged breakwater of the first three harmonics. The numerical results are found to agree well with laboratory observations [1].

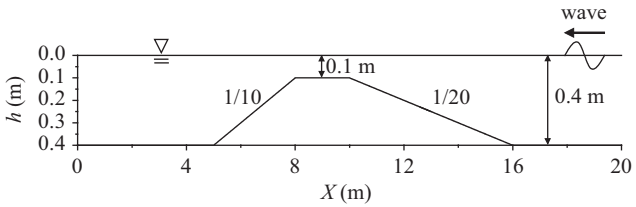

Fig. 1. Illustration of experimental setup of Beji *et al*. [1].

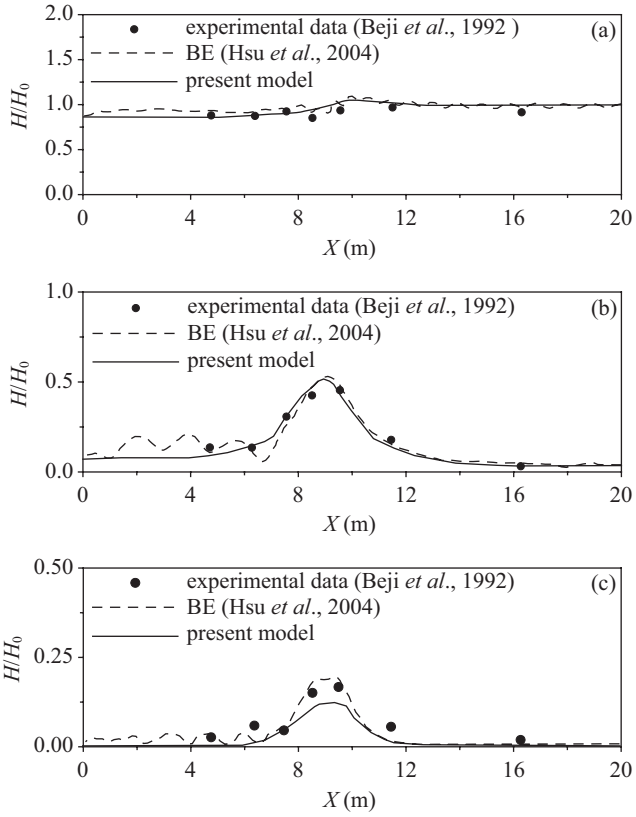

Fig. 2. Wave past a submerged bar: Comparison of wave height distributions of (a) first harmonic, (b) second harmonic, and (c) third harmonic among present model, BE model of Hsu *et al*. [16], and experimental data of Beji *et al*. [1].

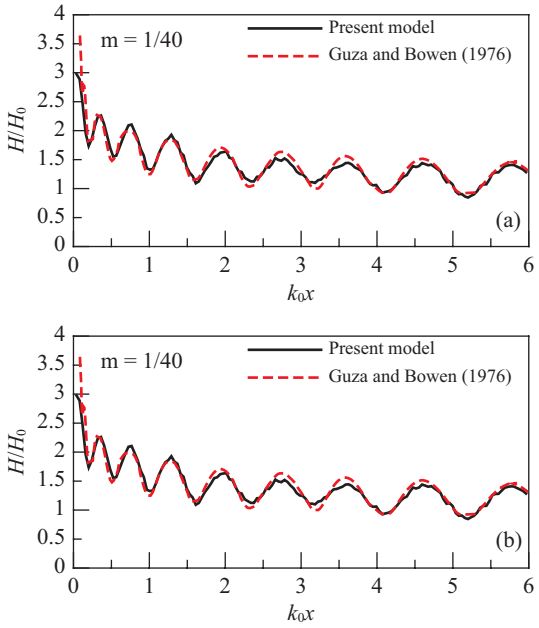

Fig. 3. Wave propagation on a sloping bed: Comparison of wave amplitude distribution of HOMSE with theory value of Guza and Bowen [13] for (a) α = 1/40 and (b) α = 1/10, respectively.

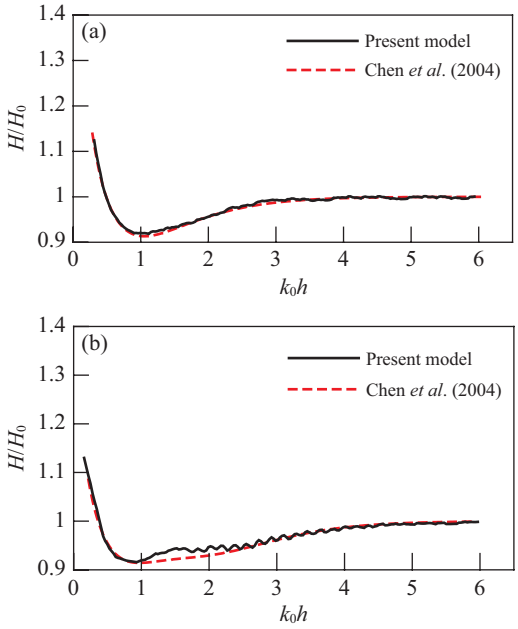

Fig. 4. Wave propagation on a sloping bed: Comparison of wave amplitude distribution of HOMSE with theory value of Chen *et al*. [9] for (a) α = 1/10 and (b) α = 1/3, respectively.

2. Wave Propagation on A Sloping Bed

HOMSE model is then applied to wave propagation on a sloping bed, whose general solution based on velocity potential was derived by Guza and Bowen [13]. Fig. 3 shows computed wave amplitude along the sloping beach for wave with H_0 = 2 m, T = 10 sec, reflection coefficient R = 0.2, and α = 1/40 and 1/10, respectively. Model prediction agrees well with theory value for both bed slopes. It is noted that partial standing waves are formed due to wave reflection from the bottom. The relative wave amplitudes vary as an envelope in the wave propagation direction. Variations of wave amplitude near shoreline are larger than that farther from shoreline because of wave shoaling and wave reflection.

In some practical applications, the reflected waves are neglected, and only progressive waves are solved for efficient calculations. Therefore, we assume variation of wave amplitude in the alongshore direction is an order of magnitude smaller than that in the onshore direction. Fig. 4 depicts comparison wave amplitude distribution of HOMSE with theory value of Chen *et al*. [9] for α = 1/10 and 1/3, respectively. As one can see, prediction of HOMSE model is close to theory value of Chen *et al*. [9].

3. Wave Propagating over An Elliptic Shoal on A Uniform Slope

Fig. 5 depicts the bathymetry of experiment of Berkhoff *et al*. [3] for wave propagating over an elliptic shoal lying on a uniform slope. Computational domain is 21.5 m × 20 m, x and y denote the axes directed to offshore and alongshore, respectively. The bathymetry h is given as

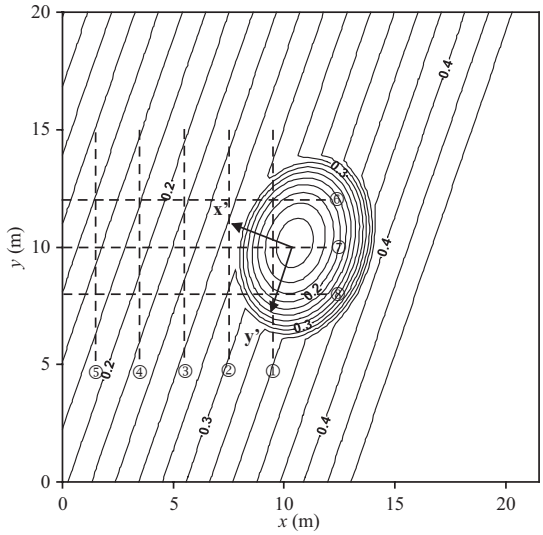

Fig. 5. Wave propagating over an elliptic shoal on a uniform slope: Bathymetry of experiment of Berkhoff *et al*. [3]. Dashed lines indicate transects of wave measurements.

$$h_s = \begin{cases} 0.45 \text{ m} & \text{for } x' < -5.82 \text{ m} \\ 0.45 - 0.02(5.82 + x') \text{ m} & \text{for } x' \geq -5.82 \text{ m} \end{cases} \tag{25}$$

$$h = \begin{cases} h_s & \text{for } (\frac{x'}{3.75})^2 + (\frac{y'}{5.0})^2 \geq 1 \\ h_s + 0.3 - 0.5\sqrt{1 - (\frac{x'}{3.75})^2 - (\frac{y'}{5.0})^2} & \text{for } (\frac{x'}{3.75})^2 + (\frac{y'}{5.0})^2 < 1 \end{cases} \tag{26}$$

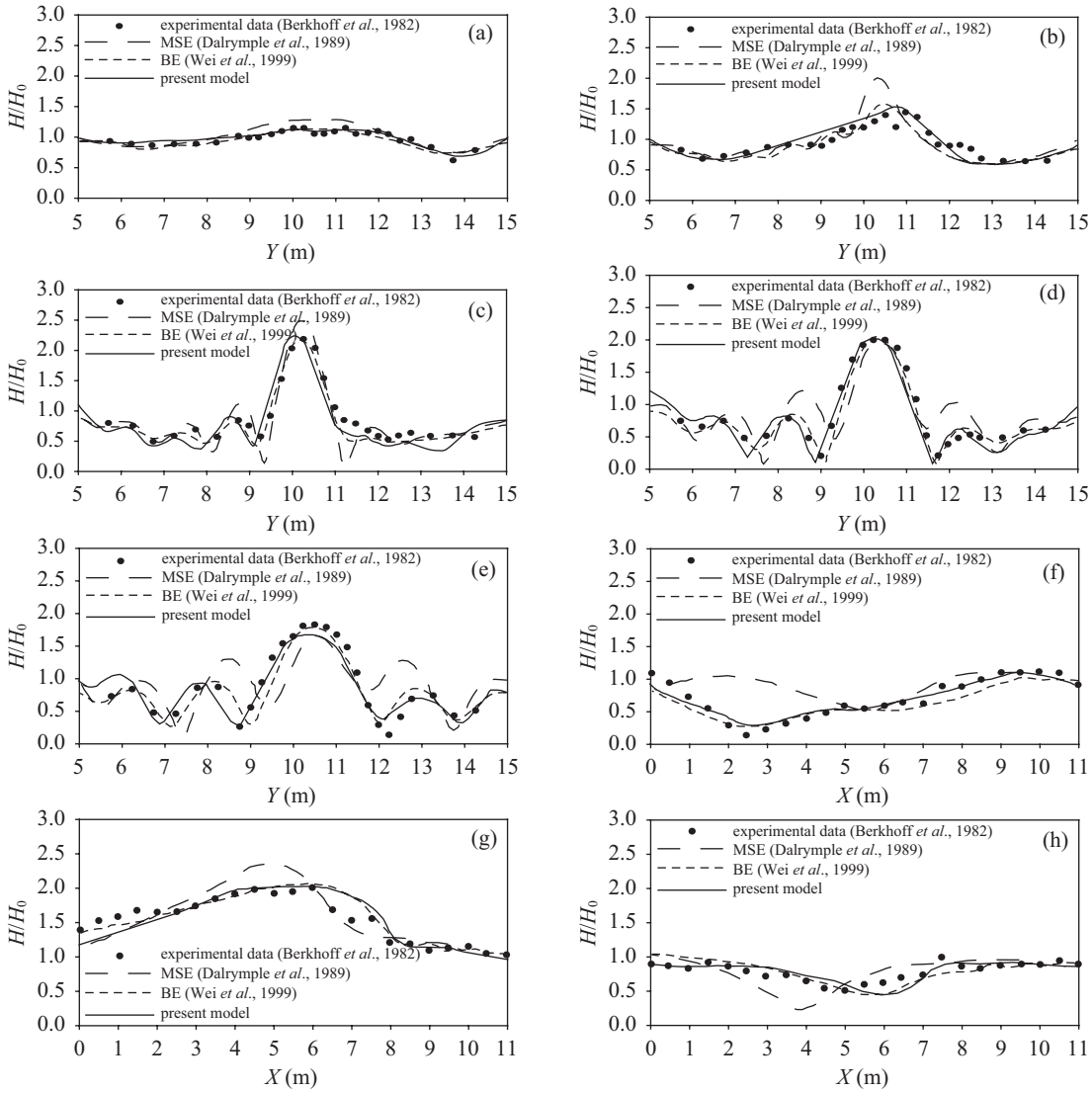

Fig. 7. Wave propagating over an elliptic shoal on a uniform slope: Comparison of wave profile of HOMSE with result of linear model of Dalrymple *et al*. [10], BE model of Wei *et al*. [23], and experiment data of Berkhoff *et al*. [3] along (a) 1st section to (h) 8th section which are shown in Fig. 5.

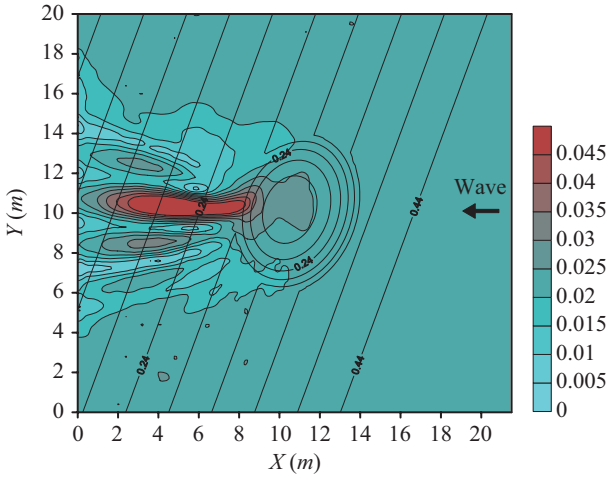

Fig. 6. Wave propagating over an elliptic shoal on a uniform slope: Wave height pattern behind the elliptical shoal.

where $x' = (x - 10.5)\cos 20° - (y - 10)\sin 20°$ and $y' = (x - 10.5)\sin 20° - (y - 10)\cos 20°$, h_s is the depth of the uniform bottom with a slope of 1/50, the deepest bottom depth is 0.45 m and the shallowest depth is 0.1332 m.

Incident wave conditions are: wave height $H_0 = 0.0232$ m and period $T = 1.0$ sec, respectively. Fig. 6 shows computed wave height pattern behind the elliptical shoal. As one can see wave refraction and diffraction occur, and it leads to dramatic increase of wave height behind the elliptical shoal. Fig. 7 shows comparison of computed dimensionless wave height distributions of HOMSE with experiment data and other numerical results on the eight chosen cross-sections which are illustrated in Fig. 5. Solid circle are experiment data of Berkhoff *et al*. [3], long dashed lines are the model prediction of the original MSE model [10], short dashed lines are simulation results of BE model [23], and the solid lines represent the computed results of HOMSE model, respectively.

Table 3. Wave propagating over an elliptic shoal on a uniform slope: Comparisons of agreement index S_f among MSE, BE, and HOMSE model, respectively.

Numerical model \ Section	1	2	3	4	5	6	7	8
Present model (HOMSE)	0.965	0.946	0.958	0.980	0.975	0.975	0.950	0.891
MSE (Dalrymple *et al*. [10])	0.850	0.839	0.958	0.872	0.701	0.453	0.775	0.867
BE (Wei *et al*. [23])	0.946	0.924	0.986	0.989	0.968	0.934	0.966	0.880

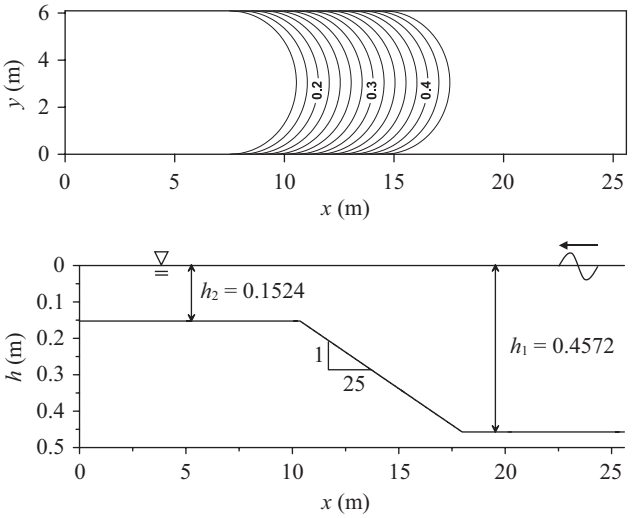

Fig. 8. Wave propagating through a semi-circular slope bottom: Sketch of experimental configuration of Whalin [24].

Computed wave height of HOMSE model is in good agreement with experiment data – It's more accurate than original MSE and comparable to BE model, in general. Table 3 sums up the agreement index between model predictions and laboratory experiment data on each section. Formula of the agreement index is given as [25]

$$S_f = 1 - \frac{\sum_{i=1}^{N} (X_i - Y_i)^2}{\sum_{i=1}^{N} \left(\left| X_i - \bar{Y} \right| + \left| Y_i - \bar{Y} \right| \right)^2} \tag{27}$$

where X_i is the computed results from numerical models, Y_i is the experimental data, $\bar{Y}$ is the average of the experimental data, and N is number of data, respectively. It is noted that discrepancy between the original MSE model [10] and experimental data is obvious, especially on sections 4 and 6. However, HOMSE model is as accurate as BE model, and more accurate than original MSE.

4. Wave Propagating through a Semicircular Slope Bottom

Wave passing through the seabed of the semicircular slope topography, which was laboratory experiment conducted by Whalin [24], is simulated. The experimental seabed is divided into three parts. The first segment is a deep-water plane bed with depth h_1 = 0.4572 m, the second seabed is the semicircular slope of α = 1/25, and the last segment is a horizontal seabed which the depth h_2 = 0.1524 m, respectively. Fig. 8 illustrates the experiment configuration, where the computation domain is 25.6 m × 6.096 m, x is the offshore coordinate and y is the alongshore coordinate, respectively. The depth function $h(x, y)$ is

Table 4. Incident wave condition and still water depth of experiment of Whalin [24].

Case	T (sec)	a_i (m)	H (m)	$k_0 h$
Case 1	1.0	0.0195	0.4572	1.922
Case 2	2.0	0.0075	0.4572	0.735

$$h(x,y) = \begin{cases} 0.4572 & \text{for } 14.93 + G < x \le 25.6 \\ 0.4572 + (10.67 - G - x)/25 & \text{for } 7.31 + G \le x \le 14.93 + G \\ 0.1524 & \text{for } x \le 7.31 + G \end{cases} \tag{28}$$

where $G = y(6.096 - y)]^{1/2}$, $0 \le y \le 6.096$.

Two incident wave conditions are considered, as shown in Table 4. Figs. 9 and 10 show computed wave harmonics of HOMSE, experiment data, and other model simulations along the centerline of the wave tank (y = 3.048 m) of Case 1 and Case 2, respectively. Solid lines are computed results of HOMSE model ($\varepsilon^i \alpha^j$, $i + j \le 3$), solid circle points are the experiment data [24], and dashed lines are the numerical simulations of Tang and Ouellet [21] ($\varepsilon^i \alpha^0$, $i \le 3$), respectively. As the waves pass through a semi-circular slope bed, water depth decreases, high-order harmonic waves are generated. Amplitude of 1st-order harmonic wave increases gradually by the effects of shoaling and focusing; Amplitude of 2nd- and 3rd-order harmonic wave also raises in the shallow water region, due to nonlinear effect. Table 5 shows the agreement index between the computed results from numerical models and laboratory experiment data. HOMSE model offers an accurate prediction for the first three wave harmonics.

IV. CONCLUSION

In the present study, a new form of the higher-order mild-slope equation (HOMSE) which describes the depth

Table 5. Wave propagating through a semi-circular slope bottom: Comparisons of agreement index S_f among MSE, BE, and HOMSE model, respectively.

Case \ Wave harmonic		First harmonic	Second harmonic	Third harmonic
1	Present model (HOMSE)	0.888	0.934	
	Tang and Ouellet [21]	0.866	0.950	
2	Present model (HOMSE)	0.978	0.971	0.897
	Tang and Ouellet [21]	0.956	0.949	0.909

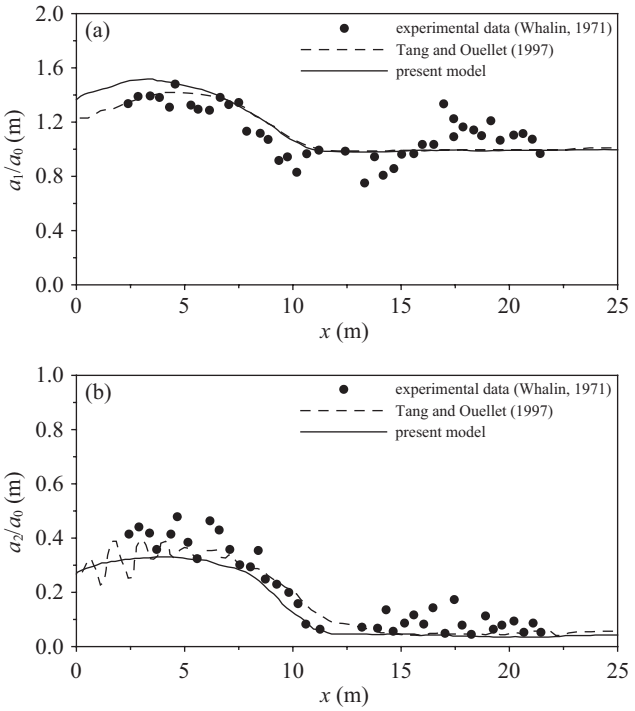

Fig. 9. Wave propagating through a semi-circular slope bottom: Comparison of wave amplitude distribution of (a) 1st harmonic and (b) 2nd harmonic of HOMSE with result of Tang and Ouellet [21], and experiment data of Whalin [24] along the center line of the wave tank. (Case 1: a_i = 0.0195 m and T = 1.0 sec)

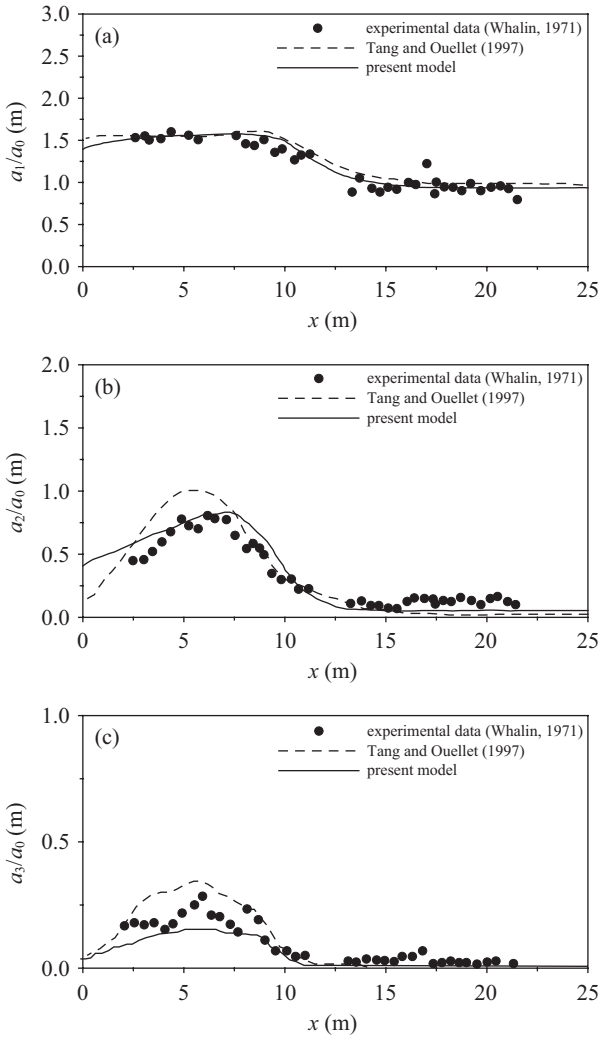

Fig. 10. Wave propagating through a semi-circular slope bottom: Comparison of wave amplitude distribution of (a) 1st harmonic, (b) 2nd harmonic, and (c) 3rd harmonic, respectively, of HOMSE with result of Tang and Ouellet [21], and experiment data of Whalin [24] along the center line of the wave tank. (Case 2: a_i = 0.0075 m and T = 2.0 sec)

function in a more accurate form is derived. Parameter of wave nonlinearity and bottom slope are included in the theoretical formulation, therefore, it can accurately predict wave propagation over a sloping beach.

HOMSE model has been verified and applied to some test cases, including propagation of a sinusoidal wave past a submerged bar, wave propagating on a sloping bed, wave propagating over an elliptic shoal on a uniform slope, and wave propagating through a semicircular slope bottom, respectively. It can accurately predict wave shoaling, refraction, diffraction, reflection, and high-order harmonics generation. Computed results show that prediction of HOMSE model agree well with experiment data. It shows the improvement of accuracy of HOMSE model compared with low-order mild-slope equation model. It's accuracy and applicability is comparable to Boussineq equations model for the cases considered.

ACKNOWLEDGMENTS

This research was supported by the National Science Council under grant number NSC96-2221-E-006-061, Taiwan, and in part by the Landmark Project of National Cheng Kung University, Taiwan.

REFERENCES

1. Beji, S., Ohyama, T., Battjes, J. A., and Nadaoka, K., "Transformation of nonbreaking waves over a bar," *Coastal Engineering*, Vol. 22, pp. 51-61 (1992).
2. Berkhoff, J. C. W., "Computations of combined refraction-diffraction," ASCE *Proceeding of the 13th International Conference Coastal Engineering*, New York, pp. 471-490 (1972).
3. Berkhoff, J. C. W., Booij, N., and Radder, A. C., "Verification of numerical wave propagation models for simple harmonic linear water waves," *Coastal Engineering*, Vol. 6, pp. 255-279 (1982).
4. Biesel, F., "Study of wave propagation in water of gradually varying depth," *Proceedings of the NBS Semicentennial Symposium on Gravity Waves*, Washington, D.C., pp. 243-253 (1951).
5. Booij, N., "A note on the accuracy of mild-slope equation," *Coastal Engineering*, Vol. 7, pp. 191-203 (1983).
6. Chamberlain, P. G. and Porter, D., "The modified mild-slope equation," *Journal of Fluid Mechanics*, Vol. 291, pp. 393-407 (1995).
7. Chen, Y. Y., Hsu, H. H., Chen, G. Y., and Hwung, H. H., "Theoretical analysis of surface waves shoaling and breaking on a sloping bottom part 2. nonlinear waves," *Wave Motion*, Vol. 43, pp. 339-356 (2006).
8. Chen, Y. Y., Hwung, H. H., and Hsu, H. H., "Theoretical analysis of surface waves propagation on sloping bottoms part 1," *Wave Motion*, Vol. 42, pp. 335-351 (2005).
9. Chen, Y. Y., Yang, B. D., Tang, L. W., Ou, S. H., and Hsu R. C., "Transformation of progressive waves propagating obliquely on gentle slope," *Journal of Waterway Port Coastal and Ocean Engineering*, Vol. 130, pp. 162-169 (2004).
10. Dalrymple, R. A., Suh, K., Kirby, J. T., and Chae, J. W., "Models for very wide-angle water waves and wave diffraction. Part 2. Irregular bathymetry," *Journal of Fluid Mechanics*, Vol. 201, pp. 299-322 (1989).
11. Davies, A. G. and Heathershaw A. D., "Surface-wave propagation over sinusoidally varying topagraphy," *Journal of Fluid Mechanics*, Vol. 144, pp. 419-443 (1984).
12. Gobbi, M. F., Kirby, J. T., and Wei, G., "A fully nonlinear Boussinesq model for surface waves. Part 2. extension to $O(kh)^4$," *Journal of Fluid Mechanics*, Vol. 405, pp. 181-210 (2000).
13. Guza, R. T. and Bowen, A. J., "Resonant interaction for waves breaking a beach," ASCE *Proceeding of the 15th International Conference Coastal Engineering*, pp. 560-579 (1976).
14. Hsu, T. W., Lin, T. Y., Wen, C. C., and Ou, S. H., "A complementary mild-slope equation derived using higher-order depth function for wave obliquely propagating on sloping bottom," *Physics of Fluids*, Vol. 18, 087106-1-14 (2006).
15. Hsu, T. W. and Wen, C. C., "On radiation boundary conditions and wave transformation across the surf zone," *China Ocean Engineering*, Vol. 15, No. 3, pp. 395-406 (2001).
16. Hsu, T. W., Yang, B. D., and Tseng, I. F., "On the range of validity and accuracy of Boussinesq-type models," *China Ocean Engineering*, Vol. 18, No. 1, pp. 93-106 (2004).
17. Lin, D. Y., *Theoretical Formulation of Higher-Order Mild-Slope Equation*, Ph.D. Thesis, Department of Hydraulics & Ocean Engineering, National Cheng Kung University, Taiwan, R.O.C. (2010).
18. Madsen, P. A., Bingham, H. B., and Liu, H., "A new Boussinesq method for fully nonlinear waves from shallow to deep water," *Journal of Fluid Mechanics*, Vol. 462, pp. 1-30 (2002).
19. Radder, A. C., "On the parabolic equation method for water wave propagation," *Journal of Fluid Mechanics*, Vol. 95, No. 1, pp. 159-176 (1979).
20. Svendsen, I. A., *The Wave Equation for Gravity Waves in Water of Gradually Varying Depth*, ISVA, Technology University of Denmark, Basic Research Progress Report, Vol. 15, pp. 2-7 (1967).
21. Tang, Y. and Oullet, Y., "A new kind of nonlinear mild-slope equation for combined refraction – diffraction of multifrequency," *Coastal Engineering*, Vol. 31, pp. 3-36 (1997).
22. Wei, G., Kirby, J. T., Grilli, S. T., and Subramanya, R., "A fully nonlinear Boussinesq model for surface waves. Part 1. Highly nonlinear unsteady waves," *Journal of Fluid Mechanics*, Vol. 294, pp. 71-92 (1995).
23. Wei, G., Kirby, J. T., and Sinha, A., "Generation of waves in Boussinesq models using a source function method," *Coastal Engineering*, Vol. 36, pp. 271-299 (1999).
24. Whalin, R. W., *The Limit of Application of Linear Wave Refraction Theory in a Convergence Zone*, Report No. H-71-3, U.S. Army Crops of Engineers Waterway Experiment Station, Vicksburg, MS (1971).
25. Willmot, C. J., "On the validation of models," *Physical Geography*, Vol. 2, No. 2, pp. 219-232 (1981).